# Photon counting three-dimensional passive sensing and object recognition

Bahram Javidi*[a], Edward Watson[b], and Seokwon Yeom[a]
[a]Dept. of Electrical and Computer Engineering, U-2157, University of Connecticut, Storrs, CT USA 06269-2157;
[b]U.S. Airforce Research Laboratories, Wright Patterson Air Force Base, Dayton, OH USA 45433

## ABSTRACT

In this keynote address, we introduce three-dimensional (3D) passive sensing using photon counting integral imaging. We investigate both linear and nonlinear matched filtering for automatic target recognition (ATR). Significant benefits of the nonlinear matched filtering with 3D integral imaging are found for ATR with a low number of photons. The discrimination capability of our system is quantified in terms of discrimination ratio (DR), Fisher ratio (FR), and receiver operating characteristic (ROC) curves. Experimental and simulation results are presented.

**Keywords:** Three-dimensional image processing; Photon counting; Integral imaging; Passive sensing; Automatic target recognition; Nonlinear matched filtering.

## 1. INTRODUCTION

The aim of automatic target recognition (ATR) is to detect and identify unknown objects in a scene and categorize them into a class [1-10]. The discrimination capability to identify targets is often challenged by uncooperative objects and noisy environments. Numerous techniques using two-dimensional (2D) image processing have been developed while there has been growing interest in three-dimensional (3D) imaging and processing [6-8]. One can find that additional benefits of 3D imaging include the ability to segment the object of interest from the background and to change the point of view of the observer with respect to the image. Many 3D imaging techniques involve some form of active illumination; the waveform that is transmitted is used to derive the range dimension of the image. However, for imaging applications in which cost and covertness are important, the use of an illumination source may not be feasible.

Photon counting is passive sensing which has been applied in many fields such as night vision, laser radar imaging, radiological imaging, and stellar imaging [11-19]. The photon counting can be binary at low light level. The advantage of the photon counting detector may be enhanced by the processing of binary photon numbers since it can be simpler and faster [12]. Photon counting techniques for 2D image recognition have been researched [12,13]. Photon counting techniques have been applied to infrared imaging and thermal imaging [14,15]. Photon counting detectors have been considered for 3D active sensing by LADAR [16-19].

Integral imaging is a 3D sensing and reconstruction (display) technique [20-23]. For recording, a micro-lenslets array generates a set of 2D elemental images on an image sensor. Each elemental image has a different perspective of the 3D scene according to the corresponding lenslet. Therefore, the image sensor records a set of projections of the 3D object from different perspectives. For reconstruction, the recorded 2D elemental images are projected through a similar micro-lens array to produce the original 3D scene. Integral imaging is passive sensing unlike holography or LADAR, which require active illumination of the scene. The application of integral imaging has been extended to object recognition and longitudinal distance estimation [24-27]. Recently, nonlinear matched filtering using photon counting integral imaging is proposed for ATR [28].

In this keynote address, we review the passive sensing and recognition of 3D objects by means of photon counting integral imaging [28]. Nonlinear matched filtering is developed for the recognition of 3D objects. The nonlinear matched filtering is performed between a reference (irradiance image) and unknown inputs (photon-limited images). We analyze the statistical properties of the nonlinear correlation normalized according to the power law of the sum of photon numbers assuming the low level of photons. Significant potentials have been found in our approach to the application of

*bahram@engr.uconn.edu; phone 1 860 486-2867; fax 1 860 486-6339

Sensors, and Command, Control, Communications, and Intelligence (C3I) Technologies for Homeland Security and Homeland Defense V, edited by Edward M. Carapezza, Proc. of SPIE Vol. 6201, 62010K, (2006)
0277-786X/06/$15 · doi: 10.1117/12.668055

ATR with a low level of photon numbers. The discrimination capability is demonstrated in terms of discrimination ratio (DR), Fisher ratio (FR), and receiver operating characteristic (ROC) curve.
In Section 2, we provide a short review of integral imaging with advantages for object recognition. In Section 3, the photon counting model is presented for the simulation of photon-limited images. Linear and nonlinear matched filtering is illustrated with performance evaluation metrics in Section 4. In Section 5, simulated photon-limited images are generated from experimentally-sensed irradiance of elemental images. These simulated images are used to verify the results presented in Section 4. Conclusions follow in Section 6.

## 2. INTEGRAL IMAGING

Techniques based on integral imaging have been considered for 3D sensing and display. During recording, we use a micro-lenslet array to sense irradiance and directional information of rays from 3D objects as shown in Fig. 1(a). Reconstruction is the reverse of the recording process. We can perform optical and numerical reconstruction from elemental images. In display, the 3D scene of the pseudoscopic real image is formed by propagating the intensity of elemental images through the lenslet array which is placed in front of the display device. The pseudoscopic real image is displayed by the rays from opposite directions but having the same irradiances as in the sensing process. The 3D display of integral imaging provides autostereoscopic images with full parallax and continuously varying viewpoints [22,23]. In the computational method, the reconstruction is processed numerically on a computer. Computational reconstruction has been researched with various techniques [26,29-31].
One advantage of integral imaging for object recognition is its capability of multiple-perspective imaging by a single shot. The depth and perspective information in the multiple perspective imaging can be utilized to build a compact 3D recognition system. In this keynote address, we assume that each lenslet in the lenslet array generates a photon-limited elemental image on a photon counting detector array as illustrated in Fig. 1(a). Multiple perspectives of photon-limited scenes are recorded according to the corresponding lenslet.

## 3. PHOTON COUNTING DETECTION MODEL

Assuming the irradiance at the detector is perfectly uniform in time and space, the probability of counting $k$ photons in a time interval $\tau$ can be shown to be Poisson distributed [32]. Although, in the case that the irradiance is not uniform, the statistics of the irradiance fluctuations must be considered, it can be shown [32] for many cases of interest (i.e. blackbody radiation in the visible, including blackbody radiation from sources as hot as the sun) that the fluctuations in irradiance are small compared to the fluctuations produced by the quantized nature of the radiation. Therefore, the probability distribution can be modeled as Poisson distribution:

$$P_d(k;x,\tau) = \frac{[a(x)\tau]^k e^{-a(x)\tau}}{k!}, \quad k = 0,1,2,..., \tag{1}$$

where $k$ is the number of counts produced by a detector centered on a position vector $x$ during a time interval $\tau$, and $a(x)$ is a rate parameter. The rate parameter can be given by:

$$a(x) = \frac{\eta P_o(x)}{h\bar{v}}, \tag{2}$$

where $\eta$ is the quantum efficiency of the detection process, $P_o$ is the optical power incident on the detector, $h$ is Plank's constant, and $\bar{v}$ is the mean frequency of the quasi-monochromatic light source. It is noted that the mean of photo-counts $n_p(x)$ can be given by:

$$n_p(x) \equiv \langle k(x) \rangle = a(x)\tau = \frac{\eta P_o(x)}{h\bar{v}}\tau, \tag{3}$$

where $\langle \cdot \rangle$ stands for the expectation operator.

It can be shown [32] that the probability of detecting a photo-event at the $i$th pixel is given by the normalized irradiance image. Since the event location for each count is an independent random variable, the mean of photo-counts at the $i$th pixel is given by:

$$n_p(x_i) = \frac{N_P S(x_i)}{\sum_{j=1}^{N_T} S(x_j)}, \tag{4}$$

where $N_P$ is a predetermined mean number of photo-counts in the entire scene; $x_i$ is the location vector of pixel $i$; $S(x_i)$ is the irradiance at pixel $i$; and $N_T$ is the total number of pixels.

To simulate photon-limited images from an irradiance image, we assume the probability of detecting more than one photon in a pixel is zero. While this assumption does place restrictions on the allowed irradiance distribution in the image, we make it in anticipation that the image will contain very few photons, i.e. $n_p(x) << 1$. If the image contains pixels whose irradiance is much larger than the mean image irradiance, then the above assumption may not be valid. In this case, $n_p(x)$ can be large enough so that the assumption $n_p(x) << 1$ is not valid even at the anticipated low-level of photons in the scene. In this case, our hypothesis could be revised to allow multiple photon detection per pixel. However for low numbers of detected photons and for scenes in which the total irradiance is distributed more evenly over the image, the binary assumption of the photon counts is valid, allowing us to use the benefits of binary imaging.

From Eq. (1), we can obtain the probability that no photon arrives at pixel $i$:

$$P(0;x_i) = e^{-n_p(x_i)}. \tag{5}$$

According to the binary assumption above, the probability that only one photon is detected:

$$P(1;x_i) = 1 - P(0;x_i) = 1 - e^{-n_p(x_i)}. \tag{6}$$

To simulate an image consisting of individual photo-counts, we generate a random number which is uniformly distributed between 0 and 1 at each pixel. If the random number is less than the probability that no photon arrives [Eq. (5)], we assume that no photon is detected, otherwise, one photon is assumed to be detected:

$$\hat{S}(x_i) = \begin{cases} 0, & \text{if } rand(x_i) \le P(0;x_i) \\ 1, & \text{otherwise} \end{cases}, \tag{7}$$

where $\hat{S}(x_i)$ is the number of the photon detected at pixel $I$, and $rand(x_i)$ stands for the random number generated for pixel $i$.

## 4. AUTOMATIC TARGET RECOGNITION USING A NONLINEAR MATCHED FILTER

We assume the photon counting is a binary image as shown in Eq. (7):

$$\hat{S}(x_i) = b_i, \qquad i = 1,\ldots,N_T, \tag{8}$$

where $b_i$ is a random number which follows Bernoulli distribution. Equivalently, one realization of a photon-limited image can be described as:

$$\hat{S}(x_i) = \sum_{k=1}^{N} \delta(x_i - x_k), \qquad i = 1,\ldots,N_T, \tag{9}$$

where $N$ is the total number of photon detection events occurred in the scene, $\delta$ is a kronecker delta function, and $x_k$ represents the position of the pixel $k$ where a photon detection event occurs. It is noted that $N$ and $x_k$ are random numbers. Matched filtering of photon-limited images estimates the correlation between the intensity images of a reference and an unknown input image obtained during the photon counting event. We define our matched filtering as the nonlinear correlation normalized with the power $v$ of the photon-limited image as shown below:

$$C_{rs}(x_j;v) = \frac{\sum_{i=1}^{N_T} R(x_i + x_j)\hat{S}(x_i)}{\left(\sum_{i=1}^{N_T} R^2(x_i)\right)^{\frac{1}{2}}\left(\sum_{i=1}^{N_T} \hat{S}(x_i)\right)^{v}} = \frac{\sum_{k=1}^{N} R(x_k + x_j)}{A\left(\sum_{i=1}^{N_T} \hat{S}(x_i)\right)^{v}}, \tag{10}$$

where $A = \left(\sum_{i=1}^{N_T} R^2(x_i)\right)^{\frac{1}{2}}$, $R$ is the radiance of the reference image which is denoted by $r$, and $s$ represents an unknown input object from which the photon-limited image $\hat{S}$ is generated. Without loss of generality, we may assume that $R(x_i)$ and $S(x_i)$ are normalized:

$$\sum_{i=1}^{N_T} R(x_i) = \sum_{i=1}^{N_T} S(x_i) = 1. \tag{11}$$

It is noted that $C_{rs}(x_j;v)$ has the maximum value at $x_j = 0$ in our experiments:

$$C_{rs}(0;v) = \max_{x_j} C_{rs}(x_j, v). \tag{12}$$

One advantage of photon counting detection is that the computational time of the matched filtering is much faster than conventional image correlation. As shown in the second term in Eq. (10) the correlation becomes merely the sum of the reference radiance at particular pixels (photon arrivals) [12].

The following first and second order statistical properties of $C_{rs}(0;0)$ have been proven in [12,13,28]:

$$\langle C_{rs}(0;0)\rangle \approx \frac{N_P}{A}\sum_{i=1}^{N_T} R(x_i)S(x_i), \tag{13}$$

$$\mathrm{var}\big(C_{rs}(0;0)\big) \approx \frac{N_P}{A^2}\sum_{i=1}^{N_T}\big\{R^2(x_i)S(x_i)[1 - N_P S(x_i)]\big\}, \tag{14}$$

where "var" denotes the variance operator.

The following statistical properties of nonlinear correlation peak $C_{rs}(0;1)$ have been proven in [28]:

$$\langle C_{rs}(0;1)\rangle \approx \frac{1}{A}\sum_{i=1}^{N_T} R(x_i)S(x_i), \tag{15}$$

$$\mathrm{var}\big(C_{rs}(0;1)\big) \approx \frac{1}{A^2}\left(\frac{1}{N_p}\sum_{i=1}^{N_T} R^2(x_i)S(x_i) - \sum_{i=1}^{N_T} R^2(x_i)S^2(x_i)\right). \tag{16}$$

The nonlinear matched filtering shows different behaviors according to $v$. When $v = 0$, both the mean [Eq. (13)] and variance [Eq. (14)] of the correlation peak $C_{rs}(0;0)$ are approximately proportional to $N_P$ since the second term including $N_P$ in Eq. (14) affects very minimally. However, the mean of $C_{rs}(0;1)$ [Eq. (15)] does not depend on the number of photons, i.e., we can theoretically achieve the same correlation value with any small number of photons. Although the variance of $C_{rs}(0;1)$ [Eq. (16)] increases when using lower number of photons, this property of photon-limited images might be beneficial for pattern recognition applications. We would like to point out that a number of filtering algorithms may be used for ATR of photon-limited images including a variety of nonlinear filters [1-6,33].

We define discrimination ratio (DR) and Fisher ratio (FR) as our performance metrics [34]:

$$DR(r,s) \equiv \frac{m_{rr}}{m_{rs}}, \tag{17}$$

$$FR(r,s) \equiv \frac{[m_{rr} - m_{rs}]^2}{\sigma_{rr}^2 + \sigma_{rs}^2}, \tag{18}$$

where $m_{rs}$ and $\sigma_{rs}$ are the sample mean and the sample standard deviation of $C_{rs}(0;v)$, respectively, which are suitable estimates for the mean and the variance. Receiver operating characteristic (ROC) curves are also illustrated in the experimental results to investigate the discrimination capability of the proposed system.

## 5. EXPERIMENTAL AND SIMULATION RESULTS

### 5.1 3D sensing with integral imaging and photon counting simulation

We use a micro-lenslet array and a pick-up camera for the recording of elemental images. The pitch of each micro-lenslet is about 1.09 mm and the focal length of each micro-lenslet is about 3 mm. The focal length and the *f*-number of the mount lens in the pick-up camera are 50 mm and 2.5, respectively. Three types of toy cars are used in the experiments as shown in Fig. 1(b). Each car is about 4.5 cm × 2.5 cm × 2.5 cm. The distance between the pick-up camera lens and the micro-lenslet array is 11.5 cm, and the distance between the micro-lenslet array and the objects is 7.5 cm.

A set of 20×24 elemental images is captured at one exposure. One set of elemental images for one object is composed of 1334×1600 pixels and the size of one elemental image is approximately 67×67 pixels. Three sets of elemental images are shown in Fig 2. The irradiance image of the reference (*r*) or the unlabeled input (*s*) corresponds to one set of elemental images captured during the pick-up process. We simulate photon-limited images using the irradiance of the elemental images as shown in Eq. (4). Equations (5) and (7) are then used to generate the photon-limited images. Several values of $N_P$, mean number of photo-counts in the entire image, are used to test the object recognition.

### 5.2 Image recognition results

We generate photon-limited images, each with a random number of photons. To compute the statistical means and variances we generate 1000 images for each car. We also vary the mean value photon numbers from 10 to 1,000. The irradiance image of car 1 [Fig. 2(a)] is used as our reference image. Figure 3(a) shows the experimental results (sample mean) of correlation coefficients and their fluctuations (error bars) when $v = 0$ with theoretical prediction in Eq. (13). Error bars stand for $m_{rs} \pm \sigma_{rs}$. The red solid line graph represents the sample mean of autocorrelation between the intensity image and photon-limited images of car 1, and the blue dotted line graph is the sample mean of cross-correlation between the intensity image of car 1 and photon-limited images of car 2, and the black dashed line graph is the sample mean of cross-correlation between the intensity image of car 1 and photon-limited images of car 3. Figure 3(b) shows the sample variance of $C_{rs}(0;0)$ with theoretical prediction in Eq. (14). Figures 4(a) and (b) show, respectively, the sample mean and the sample variance of $C_{rs}(0;1)$ with the theoretical values in Eqs. (15) and (16). As shown in Fig. 3 and Fig. 4(a), theoretical values are presented to be very close to the experimental results. Figure 4(b) shows the approximated theoretical value of the variance. The deviation from the theoretical prediction becomes larger as the number of photons decreases as shown in Fig. 4(b).

Table 1 shows the discrimination ratios defined in Eq. (17) for $C_{rs}$ (0;0) and $C_{rs}(0;1)$. There appears to be only small variation of the discrimination ratio with varying number of photo-counts. Table 2 shows the Fisher ratio defined in Eq. (18) for $C_{rs}(0;0)$ and $C_{rs}(0;1)$. Fisher ratio decreases when using a lower number of photo-counts, but for photo-counts greater than one hundred, the Fisher ratios show good separability [14,15] between the reference and false objects when $v = 1$. Fisher ratios are larger when $v = 1$ than other values since the approximated theoretical value of the variance is proportional to $1/N_P$. Figures 5 and 6 show ROC curves corresponding to cars ($r$=1, $s$=2) and cars ($r$=1, $s$=3) for $C_{rs}$ (0;0) and $C_{rs}$ (0;1), respectively. The number of photons varies from 100 to 10.

Table 1. Discrimination ratios.

| $N_P$ | | 1000 | 500 | 100 | 50 | 10 |
|---|---|---|---|---|---|---|
| $v = 0$ | $DR(1,2)$ | 1.7001 | 1.7031 | 1.6945 | 1.6678 | 1.6872 |
| | $DR(1,3)$ | 2.0247 | 2.0290 | 2.0028 | 2.0097 | 2.0238 |
| $v = 1$ | $DR(1,2)$ | 1.6987 | 1.6997 | 1.7073 | 1.6744 | 1.6867 |
| | $DR(1,3)$ | 2.0272 | 2.0262 | 2.0174 | 2.0195 | 2.0224 |

Table 2. Fisher ratios.

| $N_P$ | | 1000 | 500 | 100 | 50 | 10 |
|---|---|---|---|---|---|---|
| $v = 0$ | $FR(1,2)$ | 77.41 | 38.63 | 7.53 | 3.59 | 0.76 |
| | $FR(1,3)$ | 131.04 | 66.05 | 12.98 | 6.46 | 1.33 |
| $v = 1$ | $FR(1,2)$ | 204.14 | 105.54 | 19.90 | 9.5 | 1.77 |
| | $FR(1,3)$ | 377.83 | 191.69 | 37.72 | 18.16 | 3.5 |

## 6. CONCLUSIONS

In this keynote address, we address 3D passive sensing and object recognition using photon counting integral imaging. Micro-lenslet array generates photon-limited elemental images with multiple perspective views. Photon events are modeled with Poisson distribution. The nonlinear correlation of photon-limited images can improve the system performance to discriminate unknown 3D objects. The first and second order statistical properties of the nonlinear matched filtering output are determined. We have observed in the experiments that the output of the nonlinear correlation provides better performance than the linear matched filter in terms of discrimination ratio, Fisher ratio, and ROC curves. The presented photon counting passive 3D sensing with integral imaging seems to be robust for pattern recognition since unknown objects captured by integral imaging may be recognized with a small number of photons.

## ACKNOWLEDGEMENTS

We are thankful to Mr. Yong-wook Song and Mr. Rodrigo Ponce-Diaz's help for integral imaging experiments. We are also thankful to Mr. Seongho Song in statistics department for valuable discussion.

## REFERENCES

1. F. Sadjadi, "Improved target classification using optimum polarimetric SAR signatures," IEEE Trans. on Aerosp. Electron. Syst. 38, 38-49 (2002).
2. A. Mahalanobis, R. R. Muise, S. R. Stanfill, and A. V. Nevel, "Design and application of quadratic correlation filters for target detection," IEEE Trans. on Aerosp. Electron. Syst. 40, 837-850 (2004).
3. H. Sjoberg, F. Goudail, and P. Refregier, "Optimal algorithms for target location in nonhomogeneous binary images," J. Opt. Soc. Am. A. 15, 2976-2985 (1998).
4. H. Kwon and N. M. Nasrabadi, "Kernel RX-algorithm: a nonlinear anomaly detector for hyperspectral imagery," IEEE Trans. on Geosci. Remote Sens. 43, 388-397 (2005).
5. F. Sadjadi, ed., *Selected papers on automatic target recognition*, SPIE-CDROM, 1999.
6. B. Javidi, ed., *Image recognition and classification: algorithms, systems, and applications*, Marcel Dekker, New York, 2002.
7. B. Javidi and F. Okano, eds., *Three-dimensional television, video, and display technologies*, Springer, New York, 2002.
8. B .Javidi, ed., *Optical imaging sensors and systems for homeland security applications*, Springer, NewYork, 2006.
9. R. O. Duda, P. E. Hart, and D. G. Stork, *Pattern classification 2nd*, Wiley Interscience, New York, 2001.
10. C. M. Bishop, *Neural networks for pattern recognition*, Oxford University Press, New York, 1995.
11. E. Hecht, *Optics 4th Edition*, Addison Wesley, 2001.
12. G. M. Morris, "Scene matching using photon-limited images," J. Opt. Soc. Am. A. 1, 482-488 (1984).
13. G. M. Morris, "Image correlation at low light levels: a computer simulation," Appl. Opt. 23, 3152-3159 (1984).
14. E. A. Watson and G. M. Morris, "Comparison of infrared upconversion methods for photon-limited imaging," J. Appl. Phys. 67, 6075-6084 (1990).
15. E. A. Watson and G. M. Morris, "Imaging thermal objects with photon-counting detector," Appl. Opt. 31, 4751-4757 (1992).
16. D. Stucki, G. Ribordy, A. Stefanov, H. Zbinden, J. G. Rarity, and T. Wall, "Photon counting for quantum key distribution with Peltier cooled InGaAs/InP APDs," J. Mod. Opt. 48, 1967-1981 (2001).
17. P. A. Hiskett, G. S. Buller, A. Y. Loudon, J. M. Smith, I Gontijo, A. C. Walker, P. D. Townsend, and M. J. Robertson, "Performance and design of InGaAs/InP photodiodes for single-photon counting at 1.55 um," Appl. Opt. 39, 6818-6829 (2000).
18. L. Duraffourg, J.-M. Merolla, J.-P. Goedgebuer, N. Butterlin, and W. Rhods, "Photon Counting in the 1540-nm Wavelength Region with a Germanium Avalanche Photodiode," IEEE J. Quantum Electron. 37, 75-79 (2001).
19. J. G. Rarity, T. E. Wall, K. D. Ridley, P. C. M. Owens, and P. R. Tapster, "Single-photon counting for the 1300-1600-nm range by use of Peltier-cooled and passively quenched InGaAs avalanche photodiodes," Appl. Opt. 39, 6746-6753 (2000).
20. M. G. Lippmann, "Epreuves reversibles donnant la sensation du relief," J. Phys. (Paris) 7, 821-825 (1908).
21. H. E. Ives, "Optical properties of a Lippmann lenticulated sheet," J. Opt. Soc. Am. 21, 171-176 (1931).
22. T. Okoshi, "Three-dimensional displays," Proceedings of the IEEE 68, 548-564 (1980).
23. J.-S. Jang and B. Javidi, "Time-multiplexed integral imaging for 3D sensing and display," Optics and Photonics News 15, 36-43 (2004).
24. O. Matoba, E. Tajahuerce, and B. Javidi, "Real-time three-dimensional object recognition with multiple perspectives imaging," Appl. Opt. 40, 3318-3325 (2001).
25. Y. Frauel and B. Javidi, "Digital three-dimensional image correlation by use of computer-reconstructed integral imaging," Appl. Opt. 41, 5488-5496 (2002).
26. S. Kishk and B. Javidi, "Improved resolution 3D object sensing and recognition using time multiplexed computational integral imaging," Opt. Express 11, 3528-3541 (2003).
27. S. Yeom and B. Javidi, "Three-dimensional distortion tolerant object recognition using integral imaging," Opt. Express 12, 5795-5809 (2004).
28. S. Yeom, B. Javidi, and E. Watson, "Photon counting passive 3D image sensing for automatic target recognition," Opt. Express 13, 9310-9330 (2005).

29. H. Arimoto and B. Javidi, "Integrate three-dimensional imaging with computed reconstruction," Opt. Lett. 26, 157-159 (2001).
30. A. Stern and B. Javidi, "Shannon number and information capacity of integral imaging," J. Opt. Soc. Am. A. 21, 1602-1612 (2004).
31. M. Martínez-Corral, B. Javidi, R. Martínez-Cuenca, and G. Saavedra, "Multifacet structure of observed reconstructed integral images," J. Opt. Soc. Am. A. 22, 597-603 (2005).
32. J. W. Goodman, *Statistical optics*, (Jonh Wiley & Sons, inc., 1985), Chap 9.
33. B. Javidi, "Nonlinear joint power spectrum based optical correlation," Appl. Opt. 28, 2358-2367 (1989).
34. F. Sadjadi, ed., *Milestones in performance evaluations of signal and image processing systems*, (SPIE Press, 1993).

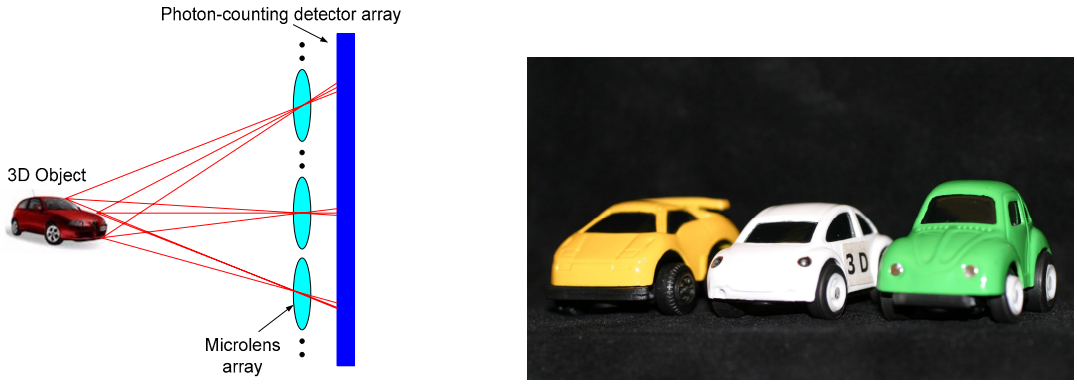


Fig. 1. (a) schematic diagram of photon counting integral imaging system, (b) three toy cars used in the experiments; car 1, 2 and 3 are shown from right to left.

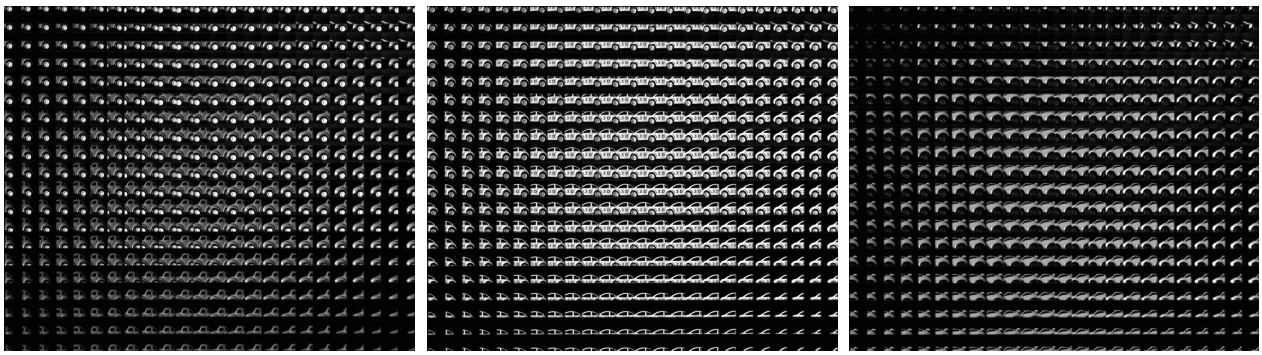

(a) (b) (c)

Fig. 2. Three sets of elemental images for irradiance information, (a) car 1, (b) car 2, (c) car 3.

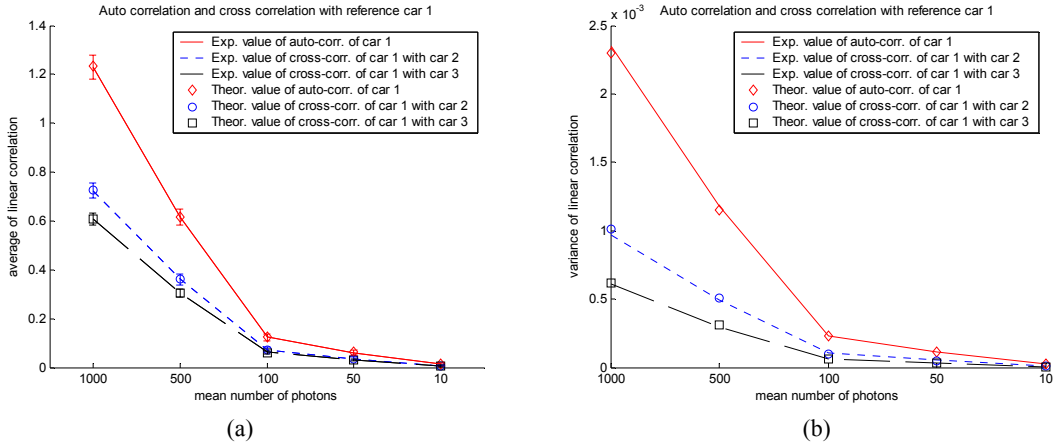


(a) (b)

Fig. 3. Mean and variance of $C_{rs}(0;0)$; (a) sample mean and theoretical prediction, (b) sample variance and theoretical prediction.

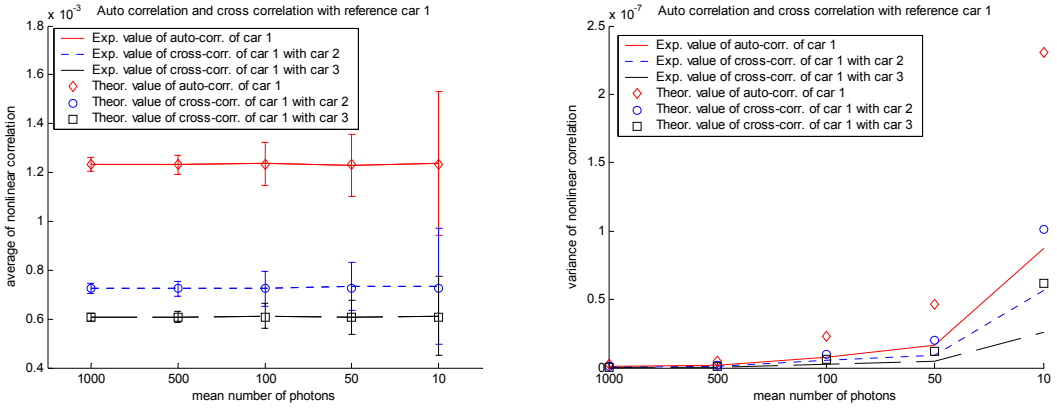


(a) (b)

Fig. 4. Mean and variance of $C_{rs}$ (0;1); (a) sample mean and theoretical prediction, (b) sample variance and theoretical prediction.

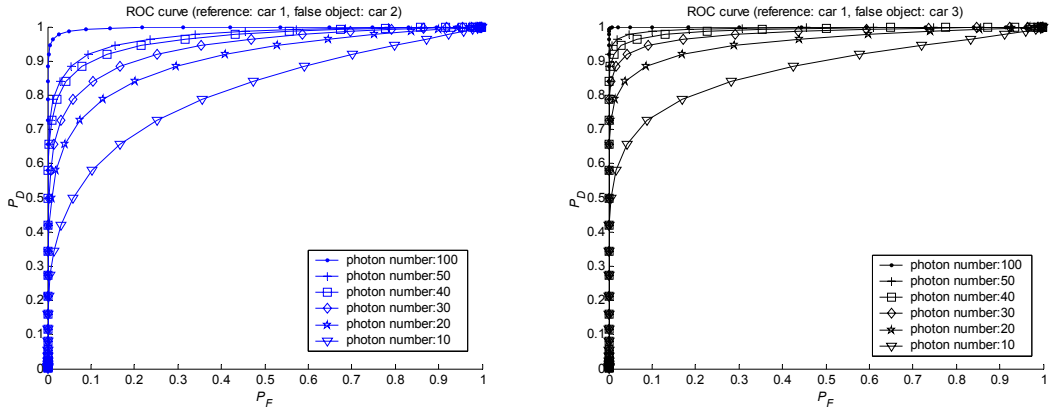


(a) (b)

Fig. 5. ROC curve of $C_{rs}$ (0;0); (a) reference is car 1 and false object is car 2, (b) reference is car 1 and false object is car 3.

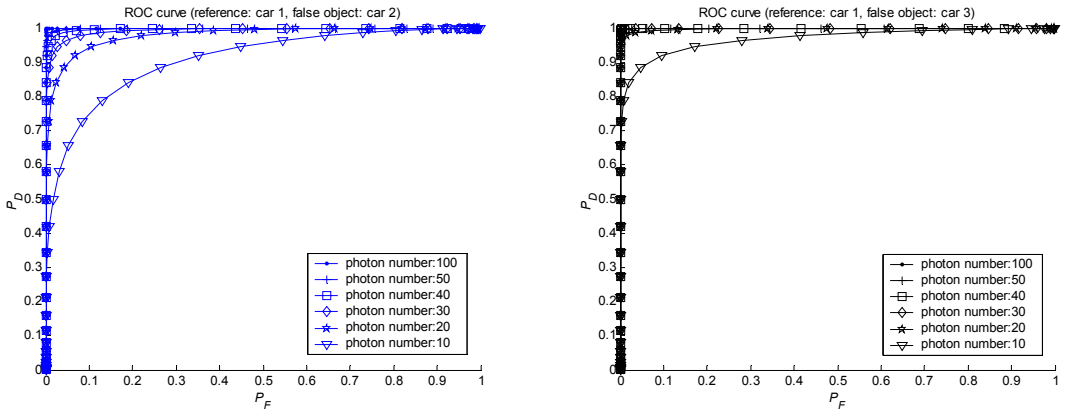


(a) (b)

Fig. 6. ROC curve of $C_{rs}$ (0;1); (a) reference is car 1 and false object is car 2, (b) reference is car 1 and false object is car 3.